Microwave-assisted depolymerization of various types of waste lignin over two-dimensional CuO/BCN catalysts

Yang Cao,[a,b] Season S. Chen,[b] Daniel C.W. Tsang,[*b] James H. Clark,[c] Vitaliy L. Budarin,[c] Changwei Hu,[d] Kevin C.-W. Wu,[e] Shicheng Zhang[*a,f]

[a] Shanghai Key Laboratory of Atmospheric Particle Pollution and Prevention (LAP3), Department of Environmental Science and Engineering, Fudan University, Shanghai 200438, China.

[b] Department of Civil and Environmental Engineering, The Hong Kong Polytechnic University, Hung Hom, Kowloon, Hong Kong, China.

[c] Green Chemistry Centre of Excellence, Department of Chemistry, University of York, York, YO10 5DD, UK.

[d] Key Laboratory of Green Chemistry and Technology, Ministry of Education, College of Chemistry, Sichuan University, Chengdu 610064, China.

[e] Department of Chemical Engineering, National Taiwan University, Taipei 10617, Taiwan.

[f] Shanghai Institute of Pollution Control and Ecological Security, Shanghai 200092, China.

Corresponding authors: E-mail: dan.tsang@polyu.edu.hk; E-mail: zhangsc@fudan.edu.cn

Abstract:

Valorization of lignin towards valuable chemicals and biofuels increases the economic viability of sustainable biorefineries. This work aimed at elucidating how the lignin structures recovered from various agricultural and industrial residues governed the downstream catalytic conversion. Three types of lignin, namely bio-enzymatic lignin (BL), organosolv lignin (OL), and Kraft lignin (KL) were fully characterized by HSQC-NMR, TGA, FTIR, and SEM to obtain a detailed description of the structures. In consideration of redox-active CuO and highly active carbon-modified boron nitride (BCN) in oxidative dehydrogenation, the two-dimensional CuO/BCN catalyst was prepared and explored in the microwave-assisted lignin conversion to improve the aromatic monomers yields. The BL achieved the highest

yield of 10 wt% monomers over the CuO/BCN catalyst after the 3rd cycle in 30 min under mild conditions (200 °C). The yields of bio-oils reached 70 wt% in 10 min when BL and OL were used as the substrate. High efficiency of microwave-assisted reaction was illustrated by comparing with that of hydrothermal reaction. This work demonstrated strong dependence of conversion efficiency on the interunit linkages and functional groups of lignin structures. The strong metal-support interaction between CuO and BCN not only facilitated lignin depolymerization *via* the promoted electron transfer, but also enhanced the stability of Cu catalysts under hydrothermal conditions. In addition, elucidation of catalyst redox evolution shed light on the role of the CuO/BCN catalyst in lignin depolymerization in recycle runs.

Keywords: lignin biorefinery; sustainable waste management; copper catalyst; oxidative dehydrogenation; metal-support interaction.

Introduction

Sustainable utilization of biological resources, especially the wastes of agriculture, forestry, and related industries, aims to address the limited fossil resource issue and present an opportunity to make biorefinery profitable.[1, 2] Valorization of lignocellulosic biomass for the production of fuels and platform chemicals has attracted increasing attention.[3, 4] The cellulose and hemicellulose fractions of biomass have been industrialized in food production, paper manufacturing (50 million tons a year), and biorefinery to produce xylose, furfural and 2nd generation biofuels.[5-8] Meanwhile, vast amounts of wastes containing abundant lignin are generated, which has been considered as a promising alternative to produce aromatic compounds with a higher energy density and potential commercial value.[9, 10] However, the mass-produced lignin residues are often underused and burned as low-grade fuel. Retrieving values from waste lignin can not only maximize the value of renewable carbon resource but also increase the economic viability of the biorefinery industry.

Separation and recovery of lignin from lignocellulosic biomass is the foremost challenging process towards effective utilization of lignin for valuable chemicals and

fuels production.[11] In view of the complex and recalcitrant structure of biomass, various fractionation technologies such as acid/base-assisted delignification, enzymatic process, and organosolv pretreatment have been developed to isolate lignin from lignocellulosic feedstocks.[12-14] Classic Kraft pulping process employs high concentration of NaOH and Na_2S solvents, where the harsh condition can modify or damage the native lignin structure.[15, 16] On the contrary, enzymatic process rarely affects the native structure of lignin owing to its mild operation condition.[12] Organosolv pretreatment utilizing different organic solvents (e.g., alcohols, organic acids, and ionic liquids) can enhance enzymatic saccharification by the removal of soluble lignin, while it inevitably leads to partial depolymerization of lignin.[12-14] Therefore, the fractionation technologies should be taken into account for the variation of lignin structure.[10, 17] Detailed analysis of interlinkages, repeat units, solubility, and thermochemical behaviour of lignin derived from diverse technologies is important for understanding how the lignin structures recovered from various biomass residues govern the downstream conversion.

Most lignin utilization strategies hinge on thermochemical conversion, mainly involving oxidative/reductive depolymerization, fast pyrolysis, and gasification.[18-22] Reductive depolymerization have shown a high activity and selectivity and could produce aromatic alkane *via* H_2 participated upgrading.[23, 24] However, the high reaction temperature (150-350 ^{o}C) and external H_2 purification would add to the cost for factory construction.[25] Oxidation of lignin is usually performed under mild condition (150-250 ^{o}C) and focuses on the production of functionalized oxygen-containing biofuels, ranging from aromatic aldehydes to carboxylic acids that are target chemicals.[26] In view of the rapid heating and energy-efficient features, microwave-assisted depolymerization can reduce the demand of external H_2 or O_2 purification and offer distinct advantages for green production of biorenewable products.[27-31]

Advanced homogeneous and heterogeneous catalysts such as transition metal-based catalysts, zeolites, and carbon-based catalysts have been widely explored for

lignin oxidation.[32-36] Among which, the Cu-based catalysts have attracted considerable interest in oxidative depolymerization of lignin due to their excellent catalytic activity and low cost.[32, 37] For example, homogeneous Cu(I) (CuCl/tetramethylpiperidine N-oxide) and Cu(II) ($CuCl_2$/polybenzoxazine) complexes can promote the cleavage of C-C and C-O bonds in the oxidation of lignin model compounds.[38, 39] Synthesized CuNiAl catalysts were found to be active in the cleavage of C-O bond for improving the yield of bio-oil during alkaline lignin conversion. However, the supported copper catalysts often suffer from metal sintering or leaching during the hydrothermal reaction.[40] The improvement of structural stability is of particular importance for sustainable catalysts. Currently, two-dimensional hexagonal boron nitride (h-BN), exhibits unique properties such as superior chemical and thermal stability and has been developed for the oxidative dehydrogenation (ODH) reaction.[41] Unprecedentedly high selectivity of ODH of propane to propene over BN has been reported, which sheds light on the active site of oxygen-terminated armchair edge of BN.[42] Due to superhydrophobic nature of h-BN, significant efforts have been made regarding modifications of the BN (e.g., heteroatom doping, vacancy defects) to achieve better dispersion and higher activity *via* tuneable physicochemical properties.[43, 44] For instance, the carbon-doped BN materials exhibited high activity in ODH of ethylbenzene and excellent oxidation resistance.[45] Hence, we intend to fabricate and investigate the modified BN supported copper catalysts for the oxidative depolymerization of lignin to achieve full utilization of waste biomass while providing new solutions to key challenges of heterogeneous catalysts.

In the present study, the CuO anchored functionalized BN catalyst (CuO/BCN) was prepared *via* soft urea strategy assisted by mechanochemical treatment and subsequent pyrolysis.[46, 47] We explored the bifunctional CuO/BCN catalyst in the alkaline oxidation of three types of lignin-rich wastes from agriculture and forestry residues with microwave radiation. Alkaline solvent is known to promote delignification by cleaving C-O bonds and enhancing solubility of lignin. Through this study, we aim to: (a) investigate the structures of lignin recovered from various methods; (b) evaluate

the catalytic activity and recyclability of CuO/BCN catalyst in the oxidative valorization of lignin to monomers and bio-oil; (c) elucidate the relationship between the structures of lignin wastes and conversion mechanisms; and (d) evaluate the influence of different heating methods by measuring monomer yields *via* hydrothermal and microwave-assisted depolymerization of lignin. Overall, utilization of lignin wastes towards target chemicals and bio-fuels might be promising through identification of lignin structure and their thermochemical reactions in microwave-assisted conversion with advanced catalysts.

2. Materials and Methods

2.1 Sources and pretreatment of lignin

Bio-enzymatic lignin wastes (BL) was obtained from Shandong Longlive Bio-Technology Co., Ltd, China. This lignin was a byproduct from xylo-oligosaccharides and bio-ethanol production from corncob. The Kraft lignin (KL, CAS number 471003) was purchased from Sigma-Aldrich. The organosolv lignin (OL) were extracted in laboratory for comparison.[48] Briefly, almond shells purchased from Hebei Chengde Lulu Co., Ltd were milled and Soxhlet-extracted by toluene/ethanol (2:1, v/v) for 24 h and dried overnight, then 30 g extracted biomass, 300 mL ethanol/water (1:1 v/v) solution and 3 mL HCl (6 M) were loaded into Parr pressure reactor and stirred at 160 °C for 10 min. The OL was precipitated by adding an excess amount of deionized water, and then the residual solid was dissolved in acetic acid-water mixture for further purification.

2.2 Preparation of BCN and CuO/BCN catalysts:

h-BN (2 g, Saint-Gobain Ceramic Materials) and urea (4 g, Sigma-Aldrich) were mixed inside a polytetrafluoroethylene milling container using a planetary ball mill at a rotation speed of 800 rpm for 8 h. A desirable amount of $Cu(NO_3)_2 \cdot 3H_2O$ and BN-urea mixtures were added into 50% ethanol/water (v/v) solution at 120 °C to keep the boiling state. Finally, the resulting gel-like product was pyrolyzed under the air atmosphere at 550 °C (heating rate: 2 °C/min) for 3 h to obtain the CuO/BCN

catalysts (CuO loading: 10 wt%). The BCN sample was prepared by a similar procedure except not adding $Cu(NO_3)_2 \cdot 3H_2O$ precursor.

2.3 Catalytic conversion of lignin under microwave irradiation:

The conditions were optimized based on previous studies.[32] In brief, we first conducted the preliminary tests of lignin depolymerization in the absence of catalyst at 160 °C, 180 °C, and 200 °C referring to the existing literature conditions and the microwave capacity (Fig. S6a). We found that lignin depolymerization at 200 °C enhanced monomer yield by 50% compared to that at 160 °C. Subsequently, NaOH concentration at a relatively low range (0.4 to 4 wt%, compared to over 10 wt% in conventional method) was evaluated to optimize the depolymerization condition (Fig. S6b). Hence, the reaction temperature at 200 °C with 4 wt% NaOH was selected for the catalytic evaluation tests. Lignin (0.2 g) was added into 10 mL solution (4 wt% NaOH and 0.1 mL of 30 wt% H_2O_2) with 0.1 g of CuO/BCN catalysts. It should be noted that the H_2O_2 was added into the NaOH solvent quickly before heating. The small amount of H_2O_2 quickly decomposed into oxygen and water during the heating process in the basic environment, as indicated by the rapidly increasing pressure in the reactor monitored by *in situ* pressure sensor. The primary role of H_2O_2 was to provide oxygen for facilitating the oxidative depolymerization of lignin. For comparison, 0.1 g of BCN and 0.03 g of $Cu(NO_3)_2 \cdot 3H_2O$ as the catalysts were also evaluated under the same condition. The mixtures were loaded in a closed vessel and heated to 200 °C with a ramp time of 2 min in an Ethos Up Microwave Reactor with a maximum power of 1800 W. The same temperature was maintained for 10-30 min under magnetic stirring. All the catalytic reactions were conducted at least in triplicate. To examine the influence of different heating methods, the hydrothermal depolymerization of lignin was conducted. The heating rate of the reactor was 10 ^{o}C/min and all other conditions were the same as above.

After the reaction, the solution pH values were adjusted to 2 with hydrochloric acid and the bio-crude oil containing aromatic monomers were extracted by using ethyl acetate for three times and subsequently analyzed by gas chromatography-mass

spectroscopy (GC-MS). The bio-oils were obtained and quantified after evaporation of ethyl acetate. For the recyclability test, the catalysts were collected by centrifugation at 3000 rpm. for 2 min, the recovered catalysts were washed with DI water and ethanol, and then dried at 60 °C over overnight.

2.4 Product identification and quantification

$$Yield\,of\,bio-oil\,(wt\,\%)=\frac{W_O}{W_L}\times 100\,\%$$

where W_O represents the weight of bio-oil extracted by using ethyl acetate, and W_L is the weight of initial lignin.

For lignin depolymerization, aromatic monomers were identified and quantitated by GC-MS (Agilent GC7890N equipped with HP-5 MS column). The conversion and yields were determined using an internal standard (decane) method on a basis of the peak area in the GC chromatogram.[18, 49]

$$C_{monomer}=\frac{W_{monomer}}{V}$$

$$Y_{monomer}=\frac{W_{monomer}}{W_{Lignin}}$$

$Y_{monomer}$: the yield of monomer based on the weight of lignin.

2.5 Characterization of catalysts and lignin:

The surface morphology and element mapping were investigated by using scanning electron microscopy with energy dispersive X-ray spectroscopy (SEM-EDX, TESCAN VEGA3 XM). Brunauer-Emmett-Teller (BET) surface areas were determined by nitrogen adsorption-desorption isotherm measurements using a gas sorption analyzer (Micromeritics Accelerated Surface Area and Porosimetry system, ASAP 2020). The crystalline structures of the catalysts were examined by X-ray diffraction analysis (XRD; Rigaku SmartLab) in a scanning range of 5-90°. Structural characteristics of lignin and obtained catalysts were determined by Fourier-transform infrared spectroscopy (FTIR, Perkin Elmer, UATR Two). Thermogravimetric analysis (TGA) was performed from 30 to 1000 °C at a heating rate of 10 °C/min under N_2

atmosphere (TGA, Rigaku Thermo Plus). The molecular weight distributions of various types of lignin were measured using gel permeation chromatography (GPC) instrument (Agilent 1260 HPLC systems) equipped with a refractive index detector (RID). The samples of 2 mg were dissolved in 1 mL THF. The H_2 temperature programmed reduction (H_2-TPR) illustrated the reducibility of catalysts. A 60 mg of sample was pretreated under the N_2 atmosphere, and then reduced in 10 vol% H_2 of N_2 (30 mL/min) at a ramp rate of 10 °C/min to 900°C.

Two-dimensional heteronuclear single quantum correlation nuclear magnetic resonance (2D HSQC NMR) spectra of various types of lignin were recorded on a Bruker AVIII 400 MHz spectrometer at 25 °C. About 80 mg of lignin was dissolved in 0.6 mL of DMSO-d6 (99.8%). The spectral widths were 11 ppm and 190 ppm for the ^{1}H- and ^{13}C-dimension, respectively. The overall amounts of aromatic units (C_9) were selected as the internal standard and quantified based on the analysis of 2D HSQC cross-signal.[50, 51] Results of structural features present in various lignin were expressed as percentage of per 100 aromatic units (Ar).

Hardwood lignin (OL): $I(C_9)units = 0.5I(S_{2,6}) + I(G_2)$

Grass lignin (BL): $I(C_9)units = 0.5I(S_{2,6}) + I(G_2) + 0.5I(H_{2,6})$

Softwood lignin (KL): $I(C_9)units = 0.5I(G_2)$

$$I_x\% = \frac{I_x}{I_{C9}} \times 100\%$$

I(C_9): the integral value of the aromatic ring.

3. Results and Discussion

3.1. Characterization of the catalyst

The 2D sheet structures of BN, BCN and CuO/BCN samples were revealed by SEM (Fig. 1). Pristine BN showed the smooth flake-like morphology (Fig. 1a), whereas reduced lateral size and rough surface were clearly observed in the BCN and

CuO/BCN samples (Fig. 1b-c). These results evidenced that ball milling can effectively exfoliate and generate defects on BN to improve its dispersibility in water.[52] Urea was adopted to introduce functional groups during ball milling and stabilize metal oxides during calcination.[46, 53] Mixing $Cu(NO_3)_2 \cdot 6H_2O$ and BN-urea under a boiling state can facilitate the formation of highly dispersed gel-like composites *via* metal-urea-BN complexation. Thermal decomposition of urea could form a thin carbon nitride coating over the BN surface, which can be applied to prevent metal agglomeration and modify the BN surface for the oxidative conversion.[46] The SEM-EDX mapping confirmed the presence of carbon nitride modifiers and highly dispersed Cu species on the catalyst surface without noticeable aggregation (Fig. 1d). The ball milling process together with soft urea strategy successfully modified the surface of BN and gave rise to a highly dispersed CuO species.

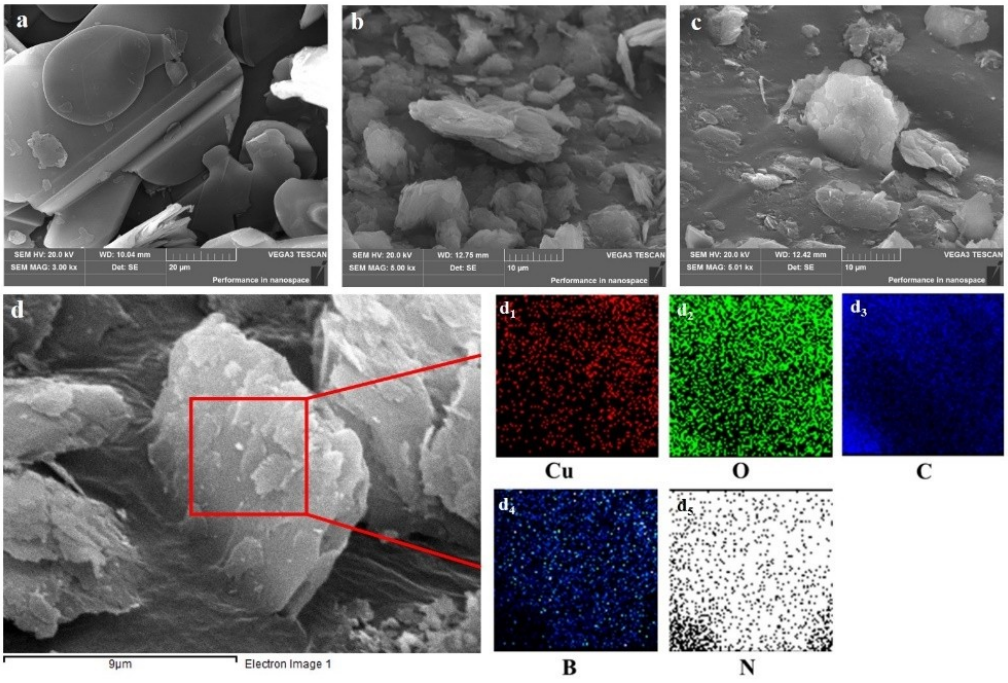

Fig. 1. SEM images of (a) BN, (b) BCN and (c) CuO/BCN catalyst and (d) elemental mapping results of CuO/BCN catalyst.

The XRD pattern verified the formation of crystalline CuO on the surface of BCN

support. The relatively low intensity of CuO phases in the XRD patterns indicated the presence of highly dispersed and small sized particles of CuO on the BCN surface. The crystallite size of CuO phase was approximately 13-17 nm calculated from XRD peaks. Four diffraction peaks centred at 26.7°, 41.6°, 50.1°, and 55.1° can be ascribed to the typical BN phases (Fig. 2a). The BCN and CuO/BCN catalysts showed that the intensities of diffraction peaks of BN phase significantly decreased. The characteristic peak at 26.7° shifted to a lower degree and became broader in the BCN as compared with the pristine BN sample, corresponding to an increase in the interplanar distance from 0.332 nm (BN) to 0.333 nm (BCN). The decreased thickness and increased lattice spacing were probably a result of milling-induced exfoliation, corroborating the presence of defects induced by carbon-heteroatom doped (Fig. S1).[54] The reflection of BN phase in CuO/BCN catalyst shifted back to the original position of BN, which may be due to the structure contraction upon the introduction of metal oxides.[55] In the FTIR spectra (Fig. 2b), two strong FTIR bands at 1380 and 760 cm^{-1} were attributed to B-N stretching and bending. Evidently, these two peaks shifted towards the higher wavenumber in contrast with that of BN, which also implied the conjugative effect of B-C-N in BCN and CuO/BCN catalysts. The Cu-O stretching at 520 cm^{-1} and 595 cm^{-1} were observed in the CuO/BCN catalyst.[56] For BCN and CuO/BCN catalysts, two small peaks at 3410 cm^{-1} and 3225 cm^{-1} could be assigned to the -OH and -NH_x groups, respectively, suggesting the presence of moisture-sensitive surface defects in the ball milled samples.

The textural properties of the catalysts were evaluated by nitrogen adsorption-desorption isotherm. The BET specific surface area of pristine BN is 2.0 m^2/g, and the corresponding pore size distribution based on the BJH model shows a primary micropore width of 1-2 nm (Table S1). After the mechanochemical treatment and calcination, the BET specific surface area of BCN increases to 45 m^2/g, and the majority of pore diameters fall into the range of 2-5 nm. The CuO/BCN catalyst shows type H_4 hysteresis loops and a range of pore sizes from 2 to 10 nm, with a slight decrease of specific surface area and volume in comparison with that of BCN

(Fig. 2c). These results suggest that the introduced CuO species are mainly loaded on catalyst surface covering partial mesopores of BCN. For the 2D catalyst, the increased surface area infers that more edges and defects derived from ball milling treatment were exposed on the BCN and CuO/BCN catalysts. The significant enhancement of specific surface area and pore volume (0.18 cm^3/g) of CuO/BCN catalyst are anticipated to accommodate more catalytic sites.

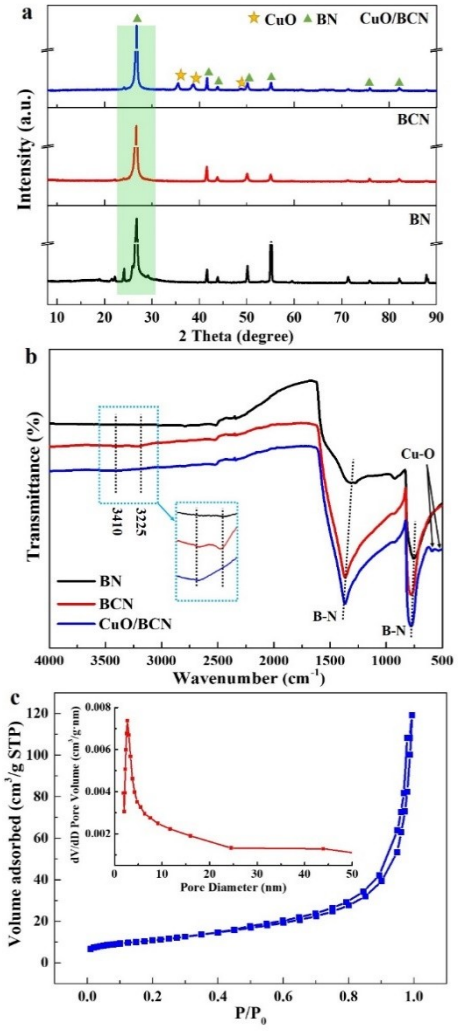

Fig. 2. (a) XRD patterns and (b) FTIR spectra of various samples, (c) N_2 adsorption-desorption isotherms of CuO/BCN catalyst.

The XPS spectra of CuO/BCN catalyst are illustrated in Fig. 3. The XPS survey spectrum showed the presence of B, C, N, O, and Cu elements. The peaks at binding

energies of 936.6 eV and 946.7 eV could be assigned to Cu $2p_{3/2}$ and Cu $2p_{1/2}$ along with shake-up satellites, indicating the oxidation state of Cu^{2+}.[57] The Cu $2p_{3/2}$ binding energy of CuO is typically reported around 933.5 eV, the higher binding energy might suggest the presence of Cu^{2+} species with a higher cationic character, indicating a strong interaction between Cu and BCN support.[58-60] Hence, the surface defects caused by ball milling together with urea can stabilize and confine CuO species on the catalyst surface. The B 1s and N 1s full width at half maxima (fwhm) peak widths were detected at 2.6 eV, which is larger than the fwhm value of pristine BN (Fig. S2). Typically, such peak broadening could be considered as a result of the superposition of multiple peaks.[61] The B 1s spectrum was deconvoluted into three peaks centred at 190.4 eV, 191.3 eV, and 192.5 eV, corresponding to B-C, B-N, and B-O bonds, respectively.[45] The primary B-N peak originated from the BN structure, and the presence of B-C bond suggested the presence of defect sites where partial B atoms could bind with C atoms. The deconvolution of N 1s showed three types of N structures, consisting of N-B (398.6 eV), N-H (399.5 eV), and N-C (400.5 eV) bonds,[62] where the N-H bonds could represent the defect sites from urea formed carbon nitride or modified BN. The spectroscopic evidence (i.e., XRD, FTIR, and XPS results) suggested that the defective surface of BN after ball milling was strongly bound with the thin carbon nitride coating. Therefore, it is likely that during the mechanochemical process, urea molecules could react with defective surface and active edges of exfoliated BN, thus possibly forming amine groups for the stabilization of CuO species. The highly dispersed CuO species and modified surface of BCN *via* forming B-C and N-C bonds may provide more active sites for the oxidation of lignin.

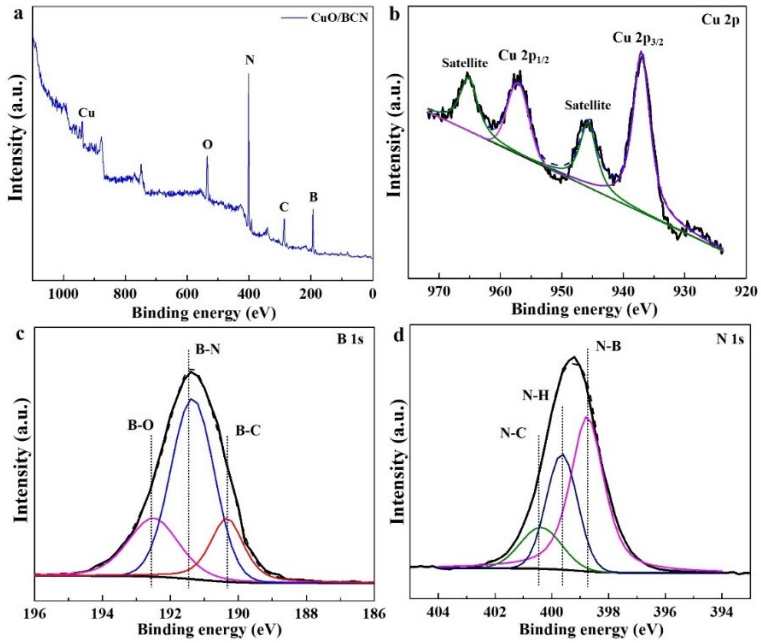

Fig. 3. XPS spectra of CuO/BCN catalyst (a) survey spectrum, (b) Cu 2p, (c) B 1s, and (d) N 1s.

3.2. Characterization of various types of lignin.

In order to identify the authentic structure of various waste lignin feedstocks and illustrate the relationship between lignin structures and depolymerization behaviour for the production of aromatic monomers and bio-oil, three typical waste lignin feedstocks (OL, BL, and KL) from biorefinery industries were selected for comparison. The particle size and surface morphology of lignin were clearly distinctive and dependent upon different extraction methods (Fig. 4a-c and Fig. S3). The SEM images showed irregular bulks of OL and BL, while KL showed uniform spherical structure, indicating destruction of the original structure and repolymerization of recovered lignin.[63] Among the three types of lignin, the OL showed the smallest particles (10 - 20 μm), followed by BL (20 μm), and KL (20 - 40 μm). In addition, the increasing weight- and number-average molecular weights (M_w and M_n) of KL listed in Table S2 illustrated the repolymerization of lignin, while the mild treatments resulted in less defined particle shapes, smaller particle sizes and molecular weights. The polydispersity index for OL and BL value were 1.48 and 1.18, respectively, which indicated good uniformity that could be beneficial for further

selective depolymerization.

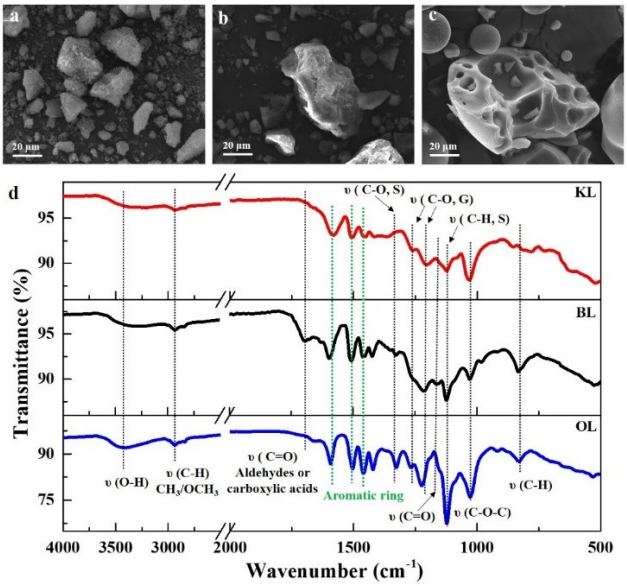

Fig. 4. SEM images of (a) OL; (b) BL and (c) KL samples; (d) FTIR spectra of various types of lignin.

The solubility, abundance in functional groups, and linkages of recovered lignin also varied. The elemental analysis showed that all three lignin samples had similar contents of fixed carbon (48-57 wt%) (Table S3). Due to the use of hydrogen sulphide in the extraction process, 3.06 wt% of sulphur was observed in KL (Table S3).[16] The slightly darker colour of KL compared to those of OL and BL samples (Fig. S4a) could be attributed to the re-condensation of lignin.[64] The modified structure of KL showed an increase in water solubility as a result of the exposed OH groups and the incorporation of sulphur species, whereas the dispersibility of OL and BL remained poor in water due to the slight change of structure under mild treatment (Fig. S4b). All lignin samples showed good dispersion in alkaline solution (4 wt% NaOH solution), which can provide effective contact between the solid catalyst and lignin for reducing mass transfer limitation.

The FTIR and NMR spectra were collected to illuminate the structures especially the interunit linkages of various lignin feedstocks recovered from different extraction methods. The FTIR showed broad signals at 3440 cm^{-1} and 2936 cm^{-1} for all three

types of lignin which can be ascribed to the stretching vibrations of O-H groups and C-H in methyl and methylene groups, respectively (Fig. 4d). A notable band at 1740 cm^{-1} was observed in BL, which can be attributed to the C=O stretching in conjugated aldehydes and carboxylic acids groups, as an evidence of partial cleavage of β-O-4 linkage resulting from steam explosion process before bio-enzymatic treatment. By contrast, such a band was absent in KL and OL. All the lignin spectra showed bands at 1590, 1505, and 1415 cm^{-1} assigned to aromatic skeletal vibrations,[65] and one centred at 1460 cm^{-1} corresponding to C-H deformation with aromatic ring vibration. Two bands at 1270 and 1215 cm^{-1} in all lignin samples represent C-O vibrations in the guaiacyl (G) unit, while 1330 and 1120 cm^{-1} were assigned to C-O and C-H vibrations in syringyl (S) unit, respectively.[48] In addition, the distinct band of C-H vibrations in the S unit observed in OL suggested an abundance of S-type of monomers. All the lignin spectra showed C-O deformation and C-H out-of-plane deformation bands at 1030 cm^{-1} and 830 cm^{-1} with different intensities,[65] indicating that the native lignin structure was affected to different extents by the extraction processes.

The 2D-HSQC analysis confirmed the presence of major lignin structures (β-O-4, β-5, β-β linkages and S/G/H units), side-chain (δC/δH 50-90/2-6) and aromatic (δC/δH 95-135/6-8) regions (Fig. 5). Three typical interunit linkages including (A) β-O-4, (B) β-5, and (C) β-β linkages were identified by C-H correlation at δC/δH 72.6/4.85 (C_α-H_α, A), 85.1/4.36 (C_β-H_β, A), 60.2/3.55 (C_γ-H_γ, A), 85.1/4.72 (C_α-H_α, B), 54.5/3.07 (C_β-H_β, B), 87.9/5.50 (C_α-H_α, C), 53.9/3.52 (C_β-H_β, C), and 62.1/3.75 (C_γ-H_γ, C).[66, 67] All lignin samples exhibited a strong signal corresponding to methoxyl (δC/δH, 55.80/3.75) in the side-chain regions. OL and BL presented more native-types of lignin with an abundant amount of β-O-4 linkages. The β-O-4 bonds were the dominant linkages in BL (grass lignin), suggesting that more native structure of lignin remained after the enzymatic process (Table 1). Typically, β-O-4 linkage accounts for 40-50%, 50-60%, and 35-45% of all linkages in softwood lignin, hardwood lignin and grass lignin, respectively.[68] The low content of β-O-4 linkage (11.2%) in OL (hardwood lignin) sample was consistent with previous studies, which reported that β-

O-4 bond could be cleaved under the organosolvolysis pretreatment.[14] By contrast, the major interunit linkages of lignin were not detectable in KL, except for the methoxyl groups. Hence, the NMR spectra verified that various extraction protocols could modify the lignin structure *via* the cleavage of β-O-4 linkages and undesired condensation reactions.

Table 1. Quantification of structures and interunit linkages of lignin.

Lignin	S[a]	G[a]	H[a]	S/G	β-O-4[a]	β-5[a]	β-β[a]	β-O-4[b]	β-5[b]	β-β[b]
OL	57.6%	42.4%	ND	1.35	11.2%	8.3%	4.0%	47.6%	35.3%	17.1%
BL	34.2%	49.2%	16.6%	0.70	19.2%	3.4%	Trace	84.9%	15.1%	Trace
KL	ND	80.3%	19.7%	-	ND	ND	ND	ND	ND	ND

[a] Results expressed per 100 Ar based on quantitative 2D-HSQC spectra. [b] Amount of specific functional group was expressed a percentage of β-O-4+β-5+β-β. ND: Not Detect.

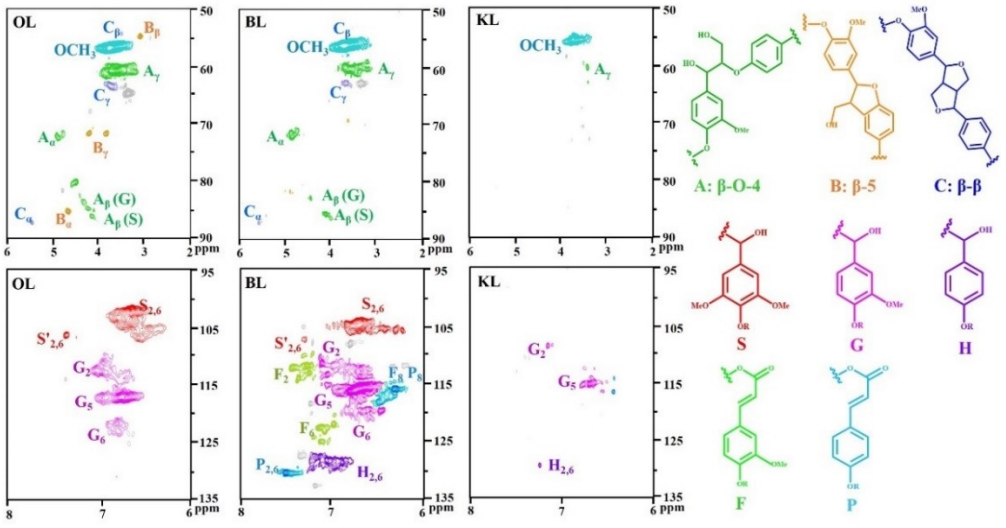

Fig. 5. Side-chain and aromatic region in 2D HSQC NMR of various lignin samples. Main substructures identified by 2D NMR: A: β-O-4 linkage; B: β-5 linkage; C: β-β linkage; S: syringyl unit; G: guaiacyl unit; H: p-hydroxyphenyl unit; F: ferulic acid unit; and P: p-coumaric acid unit.

In the aromatic region, S/G/H units were clearly distinguishable in all lignin samples. The S units were defined by δC/δH 104.3/6.65, and the signals at δC/δH

106.1/7.22 and δC/δH 128.5/7.25 were attributed to the C_α-oxidized S unit (S′) and $C_{2,6}$-$H_{2,6}$ aromatic of H unit, respectively. The G units showed different correlations at δC/δH 112.1/7.09 (C_2-H_2), 116.2/6.92 (C_5-H_5), and 120.0/6.80 (C_6-H_6). Additionally, p-coumaric acid (P) and ferulic acid (F) were detected in the spectra of BL sample, as discussed in the FTIR results.[67] The presence of P and F signals was attributed to the enzymatic delignification enhanced by steam explosion pretreatment. As shown in Table 1, the higher S/G ratio in OL than that in BL, i.e., more S units in OL, was consistent with the primary unit of hardwood lignin. Theoretically, a higher amount of S-type lignin units is favourable for the formation of β-O-4 linkage and facilitates the yield of aromatic monomer. In G/S-rich BL and G-dominant KL, the exposed C_5 position in G unit may be prone to fast monomer coupling again *via* re-condensed C-C bond during the subsequent depolymerization process. The observed difference in monolignol distribution may influence the effectiveness of depolymerization of lignin.

The TGA measurements showed that oxygen-containing functional groups (e.g., OCH_3, OH, and COOH) and various linkages in lignin are associated with different bond energies in lignin and corresponded to different cleavage temperatures.[69, 70] As shown in Fig. 6a, the weight loss of OL, BL, and KL samples was 68.2%, 69.7%, and 49.5%, respectively. The KL sample showed the highest char residue, indicating that more stable and condensed structure formed via C-C bond repolymerization during the extraction process. These results also corroborated with the structure identification by FTIR and NMR analysis. As shown in Fig. 6b, OL and BL rich in β-O-4 linkages decomposed at a lower temperature than KL due to the lower bond energies of C-O linkages in comparison to those of C-C bonds. Therefore, preserving the native structure of lignin with abundant β-O-4 linkage is possibly conducive to catalytic conversion at a lower temperature.[65] The native-like structure of OL and BL can provide a higher possibility for achieving a low-temperature selective conversion of lignin.

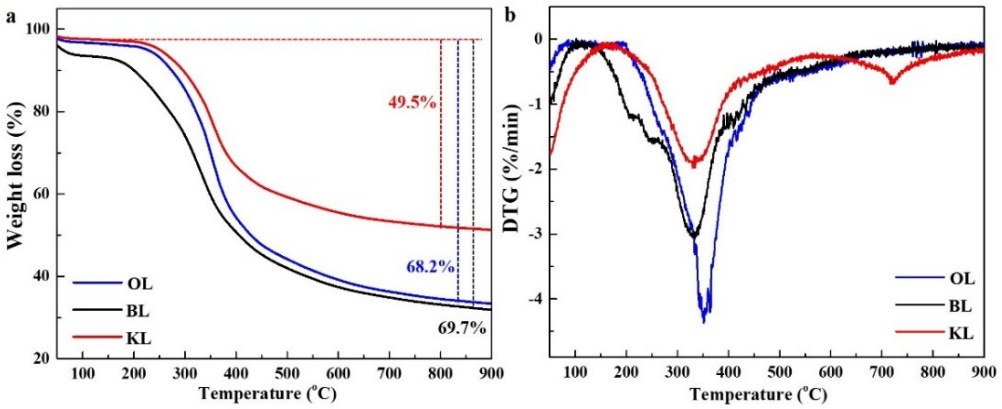

Fig. 6. (a) TGA and (b) DTG profiles of three types of lignins.

3.3. Depolymerization of lignin

The three types of lignin feedstocks showed totally different monomer distributions and yields under microwave-assisted oxidative depolymerization, highlighting the significance of lignin structure in its downstream conversion. The yields of aromatic monomers and bio-oil were greatly improved in the presence of CuO/BCN catalyst, while the product distribution was not much different than the control without catalysts (Fig. 7a). The main monomers (aromatic compounds 1-9) produced during lignin depolymerization are displayed in Fig. S5 and Table 2, consisting of vanillin (6), syringaldehyde (8), acetosyringone (9), as well as other phenols and aromatic ketones. Higher contents of aromatic monomers obtained from BL and OL depolymerization were attributed to the relatively abundant β-O-4 linkages preserved in the lignin structure, as supported by the 2D NMR analyses and TG results. In comparison, the relatively low monomer yield from KL reflected the known difficulty in valorization of the lignin waste from widely used industrial process because of repolymerized C-C bonds in the modified structure. In addition, catalytic conversion of BL over both BCN and $Cu(NO_3)_2$ showed an increase in monomer yields (Fig. S7). The modified BCN could induce unique electronic structures and provide more active sites for promoting the catalytic performance, while dispersed CuO under alkaline condition at 200 °C was also active for lignin depolymerization.[45] A combination of BCN and CuO species in the catalyst showed synergistic effects to enhance lignin

depolymerization, which highlights the promotional effect of strong metal-support interaction on the catalytic performance, as discussed in the section on XPS analysis.

Table 2. The yield[a] of aromatic monomers from depolymerization[b] of various lignin.

Entry	1 H	2 G	3 G	4 G	5 S	6 G	7 G	8 S	9 S	Total
OL 10 min	-	-	-	-	0.25	1.07	0.26	2.49	0.58	4.49
OL 30 min	-	0.19	-	-	0.37	1.78	0.40	3.50	1.07	7.32
BL 10 min	-	0.21	0.58	0.33	0.11	0.93	0.23	1.43	2.19	6.02
BL 30 min (1^{st})	0.11	0.48	0.37	0.13	0.61	2.34	0.76	2.54	2.05	9.37
KL 10 min	-	0.17	-	-	-	2.96	0.47	-	-	3.61
KL 30 min	-	0.97	-	-	-	3.34	0.68	-	-	5.08
BL 30 min (2^{nd})	0.12	0.38	0.45	0.13	0.81	2.27	0.58	2.47	1.94	9.16
BL 30 min (3^{rd})	0.18	0.64	0.22	0.17	1.30	2.36	0.66	2.25	2.14	10.00

[a] wt%, based on the initial lignin. [b] Reaction conditions: 10 mL solution, 0.1 g CuO/BCN catalyst.

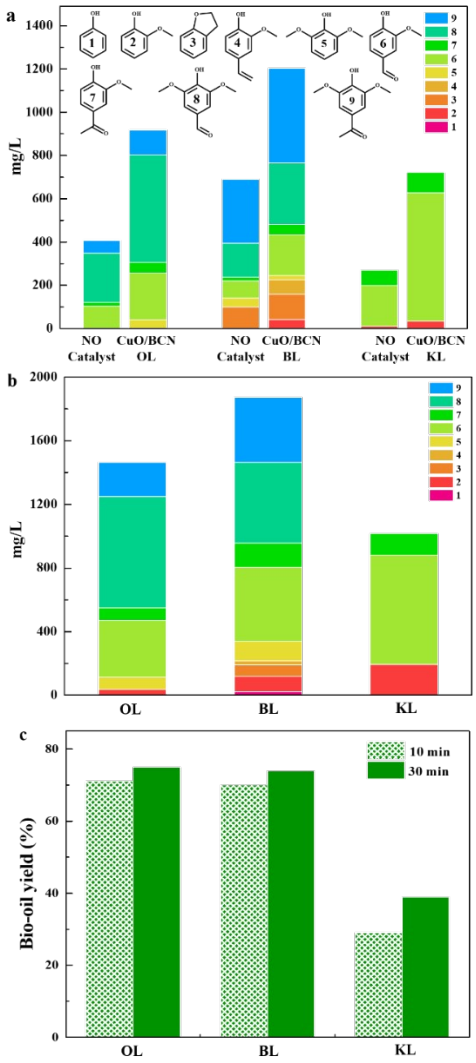

Fig. 7. Monomeric yields at (a) 10 min and (b) 30 min, and (c) yields of bio-oil from depolymerization of three types of lignin. Reaction conditions: 200 ºC, 0.2 g lignin, 10 mL solution and 0.1 g CuO/BCN catalyst.

As the reaction time increased from 10 to 30 min, the monomer yields significantly increased (Fig. 7b), while the growth of bio-oil was marginal (less than 10%) (Fig. 7c). The total yield of monomers from BL reached up to 9.4 wt% (1865 mg/L) in 30 min, which was much higher than the monomer yield from KL (5.1 wt%). These results demonstrated fast depolymerization of lignin under microwave radiation. Although the content of β-O-4 linkages was much less in OL than that in BL, the higher S/G ratio in OL may mitigate the formation of inactive C-C bonds and increase monomer yields mainly consisting of S-type monomers.[71] Higher bio-oil yields could

be achieved from the conversion of BL (73%) and OL (74%), as compared to that from KL (39%). The spent CuO/BCN catalyst after the conversion of KL was analyzed by XRD (Fig. S8), where no sulphur-containing species was detected on the catalyst surface. This result confirmed that the lower yield of monomer and bio-oil from KL conversion mainly resulted from its inert structure rather than catalyst deactivation by sulphur. These results revealed that more native-like lignin structures preserved in the feedstocks (such as BL and OL) are favourable for higher product yields of oxidative depolymerization, and the CuO/BCN catalysts are effective for the production of aromatic monomers. To examine the influence of different heating methods, the hydrothermal and microwave-assisted depolymerization of lignin were performed for comparison (Fig. S9). Microwave energy could homogeneously heat the whole biomass which is important for processing poorly thermal-conducting feedstocks. Rapid heating of the substrates can shorten the reaction time and prevent over-reaction of the obtained products. The results further confirmed synergistic effects of microwave radiation on the lignin depolymerization towards high yield and product selectivity.

In view of the high yields of monomers and bio-oil, the recyclability test of CuO/BCN catalyst was conducted for oxidative depolymerization of BL. The high yields of bio-oil were maintained after three cycles (Fig. S10). The results indicated that the CuO/BCN catalyst had no apparent loss of activity in the three cycles (Fig. 8a). Nevertheless, the monomer yields slightly increased to 10 wt% in the 3rd cycle. The XRD patterns showed that different redox dynamics were involved during the oxidative reactions. The CuO species were the only detectable Cu species observed in the fresh CuO/BCN catalyst (Fig. 2a), while Cu_2O species appeared after the 1st cycle due to partial reduction of CuO (redox cycle: CuO-Cu_2O) (Fig. 8b). After the 2nd cycle, the peak intensity of Cu_2O species decreased and metallic Cu phase was formed (redox cycle: Cu_2O-Cu_2O/Cu). After the 3rd cycle, no Cu_2O phase were detected, suggesting the transformation of Cu_2O to Cu species. The slightly improved yields in the 3rd recycle run might be attributed to the stronger redox capability of Cu_2O/Cu pair

as reported by previous studies.[32, 72, 73]

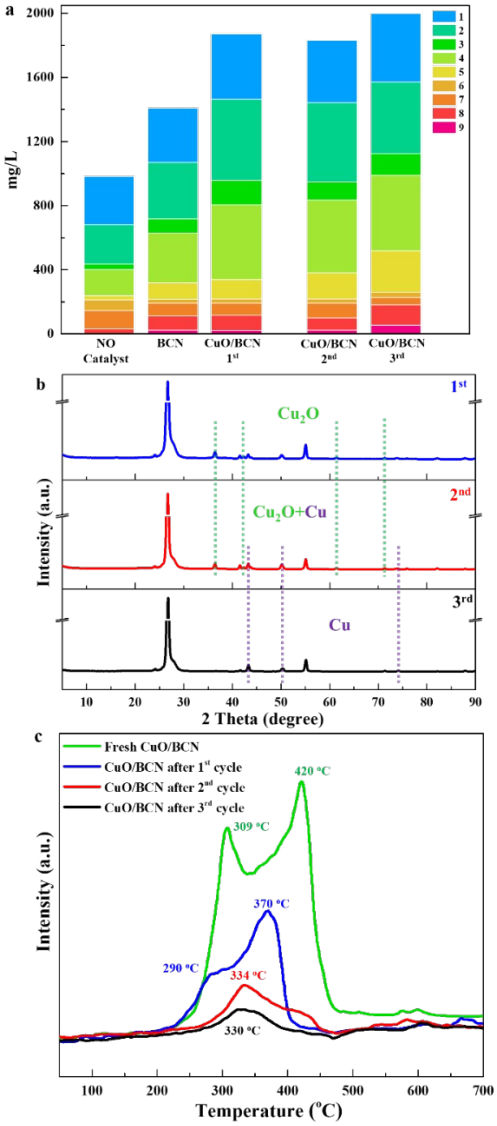

Fig. 8. (a) Recyclability test for the depolymerization of BL over CuO/BCN catalyst. Reaction conditions: 200 °C, 0.2 g BL, 10 mL solution and 0.1 g catalyst, 30 min. (b) XRD patterns, and (c) H_2-TPR profiles of the fresh and recovered catalysts after each cycle.

Furthermore, H_2-TPR profiles illustrated the surface interaction between various CuO_x species and BCN support (Fig. 8c). In fresh CuO/BCN catalyst, two reduction peaks can be distinguished at 309 °C and 420 °C. The peak at the lower temperature corresponded to the reduction of highly dispersed CuO phase, and such kind of Cu species could be readily reducible.[74, 75] The peak at the higher temperature (420 °C)

represented bulk CuO which had weaker interaction with the BCN surface. The peak decreasing from 309 °C to 290 °C indicated that a large amount of highly dispersed CuO species could participate in the oxidative reaction and be reduced in the first cycle, while the peak decreasing from 420 °C to 370 °C represented the reduction of bulk CuO.[74] The total intensity and temperature of reduction peaks decreased gradually after the second and third cycles, implying the formation of metallic Cu, which is consistent with the XRD patterns. To further shed light on redox evolution of the CuO/BCN catalyst during lignin depolymerization, a comparative reaction was conducted under the same condition in the absence of lignin (200 °C, 10 mL solution, 0.1 g catalyst, 30 min). The XRD patterns (Fig. S11) showed that CuO species were not reduced in this comparative test. These results demonstrated CuO could act as the solid oxidant during the selective oxidation of lignin.[76] The SEM images and EDX mapping of the recovered catalysts after the 3rd cycle (Fig. S12) showed similar structure to the fresh CuO/BCN catalyst and highly dispersed Cu species, illustrating superior hydrothermal stability of the catalyst and strong metal-support interaction to inhibit Cu aggregation during the oxidative depolymerization of lignin.

In light of the above experimental results, possible reaction mechanisms are proposed for the oxidation depolymerization of native lignin (β-O-4 linkage) over the CuO/BCN catalyst in this study (Scheme 1). The selective cleavage of C_α-C_β and C_β-O bonds was the most commonly recognized pathway.[77] Typically, the β-O-4 alcohol could be oxidized to β-O-4 ketone over the CuO/BCN surface under alkaline condition, and the formation of ketone intermediates could lower the C_β-O bond energy for the subsequent depolymerization (Step I).[78] The C_β-O bond cleavage facilitated the production of acetovanillone (7) and acetosyringone (9), while the yields of vanillin (6) and syringaldehyde (8) were significantly promoted by CuO/BCN catalyst; thus, the C_α-C_β cleavage might contribute to the production of aldehydes through retro-aldol reaction (Step II). Meanwhile, the Cu(II) species were reduced to Cu(I) in the absence of sufficient oxygen. The oxidative capability of copper-based catalysts on the activation of C-C bond was consistent with previous

studies,[38, 39] whereas the modified BN support and the strong metal-support interaction could promote the catalytic conversion of electron-rich aromatic substrates and intermediates. Therefore, the synergistic effect of redox-active CuO and active modified BCN support enabled efficient oxidative depolymerization of lignin.

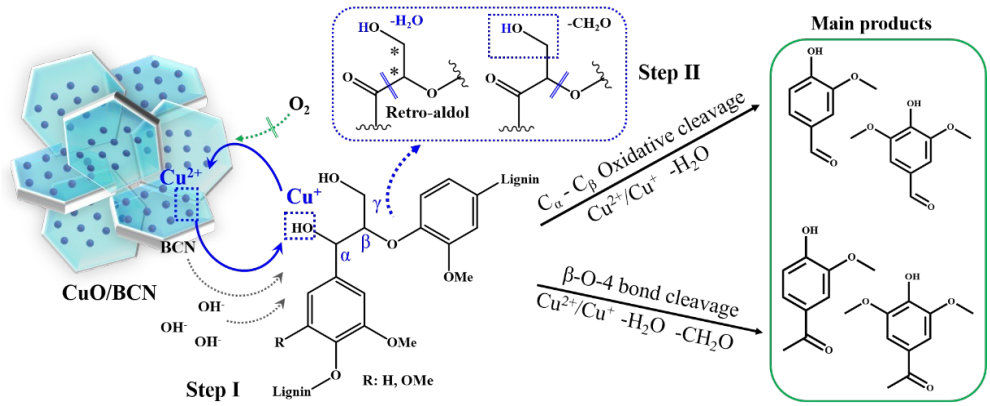

Scheme 1. Proposed reaction mechanisms for the oxidation of native type lignin.

4. Conclusions

In this work, microwave-assisted depolymerization of lignin derived from various fractionation methods was conducted over CuO/BCN catalyst. The aromatic monomers yield from lignin containing more native structures (e.g., BL and OL) could reach up to 10 wt% in 30 min, which was twice as high as that of KL with significantly modified structure. The CuO/BCN catalyst showed synergistic advantage of metal-support interaction of redox-active CuO and carbon-modified BN support for the oxidative depolymerization of lignin. Overall, these results highlight the importance of green and energy-efficient approach for achieving full utilization of waste lignin with adequate biomass fractionation protocols.

Acknowledgements

This study was supported by the International Cooperation Project of Shanghai Municipal Science and Technology Commission (No. 18230710700), National Key Research and Development Program of China (No. 2017YFC0212205), National Natural Science Foundation of China (No. 21876030), Royal Society International

Exchanges 2016 Round 2 - IE160441, Hong Kong Research Grants Council (PolyU 15217818), and Hong Kong International Airport Environment Fund (Phase 2).

References

1. Z. Sun, G. Bottari, A. Afanasenko, M. C. A. Stuart, P. J. Deuss, B. Fridrich and K. Barta, *Nat. Catal.*, 2018, 1, 82-92.
2. S. Y. Lee, H. U. Kim, T. U. Chae, J. S. Cho, J. W. Kim, J. H. Shin, D. I. Kim, Y.-S. Ko, W. D. Jang and Y.-S. Jang, *Nat. Catal.*, 2019, 2, 18-33.
3. J. Remón, J. Randall, V. L. Budarin and J. H. Clark, *Green Chem.*, 2019, 21, 284-299.
4. L. Petridis and J. C. Smith, *Nat. Rev. Chem.*, 2018, 2, 382-389.
5. L. Wang, R. Templer and R. J. Murphy, *Energy Environ.Sci.*, 2012, 5, 8281.
6. Y. Li, P. Liu, J. Huang, R. Zhang, Z. Hu, S. Feng, Y. Wang, L. Wang, T. Xia and L. Peng, *Green Chem.*, 2018, 20, 2047-2056.
7. I. K. M. Yu and D. C. W. Tsang, *Bioresour. Technol.*, 2017, 238, 716-732.
8. I. K. M. Yu, X. Xiong, D. C. W. Tsang, L. Wang, A. J. Hunt, H. Song, J. Shang, Y. S. Ok and C. S. Poon, *Green Chem.*, 2019, 21, 1267-1281.
9. M. Talebi Amiri, G. R. Dick, Y. M. Questell-Santiago and J. S. Luterbacher, *Nat. Protoc.*, 2019, 14, 921-954.
10. E. M. Anderson, M. L. Stone, R. Katahira, M. Reed, W. Muchero, K. J. Ramirez, G. T. Beckham and Y. Roman-Leshkov, *Nat. Commun.*, 2019, 10, 2033.
11. S. Kasakov, H. Shi, D. M. Camaioni, C. Zhao, E. Baráth, A. Jentys and J. A. Lercher, *Green Chem.*, 2015, 17, 5079-5090.
12. Z. Zhang, M. D. Harrison, D. W. Rackemann, W. O. S. Doherty and I. M. O'Hara, *Green Chem.*, 2016, 18, 360-381.
13. C. G. Yoo, M. Li, X. Meng, Y. Pu and A. J. Ragauskas, *Green Chemistry*, 2017, 19, 2006-2016.
14. X. Ouyang, X. Huang, B. M. S. Hendriks, M. D. Boot and E. J. M. Hensen, *Green Chem.*, 2018, 20, 2308-2319.
15. C. S. Lancefield, H. L. J. Wienk, R. Boelens, B. M. Weckhuysen and P. C. A. Bruijnincx, *Chem. Sci.*, 2018, 9, 6348-6360.
16. C. Gioia, G. Lo Re, M. Lawoko and L. Berglund, *J. Am. Chem. Soc.*, 2018, 140, 4054-4061.
17. A. Rahimi, A. Ulbrich, J. J. Coon and S. S. Stahl, *Nature*, 2014, 515, 249-252.
18. M. Wang, X. Zhang, H. Li, J. Lu, M. Liu and F. Wang, *ACS Catalysis*, 2018, 8, 1614-1620.
19. T. Kleine, J. Buendia and C. Bolm, *Green Chem.*, 2013, 15, 160-166.
20. S. Kudo, Y. Hachiyama, Y. Takashima, J. Tahara, S. Idesh, K. Norinaga and J.-i. Hayashi, *Energy Fuels*, 2013, 28, 76-85.
21. W. Wang, M. Wang, J. Huang, X. Zhao, Y. Su, Y. Wang and X. Li, *Bioresour. Technol.*, 2019, 278, 464-467.
22. L. Cao, C. Zhang, H. Chen, D. C. W. Tsang, G. Luo, S. Zhang and J. Chen, *Bioresour. Technol.*, 2017, 245, 1184-1193.
23. E. M. Anderson, M. L. Stone, M. J. Hülsey, G. T. Beckham and Y. Román-Leshkov, *ACS Sustainable Chem. Eng.*, 2018, 6, 7951-7959.

24. M. L. Stone, E. M. Anderson, K. M. Meek, M. Reed, R. Katahira, F. Chen, R. A. Dixon, G. T. Beckham and Y. Román-Leshkov, *ACS Sustainable Chem. Eng.*, 2018, 6, 11211-11218.
25. C. Zhang, C. Jia, Y. Cao, Y. Yao, S. Xie, S. Zhang and H. Lin, *Green Chem.*, 2019, 21, 1668-1679.
26. J. Dai, G. N. Styles, A. F. Patti and K. Saito, *ACS Omega*, 2018, 3, 10433-10441.
27. S. S. Chen, T. Maneerung, D. C. W. Tsang, Y. S. Ok and C.-H. Wang, *Chem. Eng. J.*, 2017, 328, 246-273.
28. S. S. Chen, I. K. M. Yu, D.-W. Cho, H. Song, D. C. W. Tsang, J.-P. Tessonnier, Y. S. Ok and C. S. Poon, *ACS Sustainable Chem. Eng.*, 2018, 6, 16113-16120.
29. I. K. M. Yu, D. C. W. Tsang, A. C. K. Yip, A. J. Hunt, J. Sherwood, J. Shang, H. Song, Y. S. Ok and C. S. Poon, *Green Chem.*, 2018, 20, 2064-2074.
30. I. K. M. Yu, X. Xiong, D. C. W. Tsang, Y. H. Ng, J. H. Clark, J. Fan, S. Zhang, C. Hu and Y. S. Ok, *Green Chem.*, 2019, DOI: 10.1039/c9gc00734b.
31. L. Cao, I. K. M. Yu, D. W. Cho, D. Wang, D. C. W. Tsang, S. Zhang, S. Ding, L. Wang and Y. S. Ok, *Bioresour. Technol.*, 2019, 273, 251-258.
32. R. Panyadee, P. Posoknistakul, W. Jonglertjunya, P. Kim-Lohsoontorn, N. Laosiripojana, B. M. Matsagar, K. C. W. Wu and C. Sakdaronnarong, *ACS Sustainable Chem. Eng.*, 2018, 6, 16896-16906.
33. B. Sedai, C. Díaz-Urrutia, R. T. Baker, R. Wu, L. A. P. Silks and S. K. Hanson, *ACS Catal.*, 2013, 3, 3111-3122.
34. A. K. Deepa and P. L. Dhepe, *ACS Catal.*, 2014, 5, 365-379.
35. M. Oregui-Bengoechea, N. Miletić, W. Hao, F. Björnerbäck, M. H. Rosnes, J. S. Garitaonandia, N. Hedin, P. L. Arias and T. Barth, *ACS Sustainable Chem. Eng.*, 2017, 5, 11226-11237.
36. X. Xiong, I. K. M. Yu, L. Cao, D. C. W. Tsang, S. Zhang and Y. S. Ok, *Bioresour. Technol.*, 2017, 246, 254-270.
37. Y. Shao, K. Sun, Q. Li, Q. Liu, S. Zhang, Q. Liu, G. Hu and X. Hu, *Green Chem.*, 2019, 21, 4499-4511.
38. B. Sedai, C. Díaz-Urrutia, R. T. Baker, R. Wu, L. A. P. Silks and S. K. Hanson, *ACS Catal.*, 2011, 1, 794-804.
39. X. Ren, P. Wang, X. Han, G. Zhang, J. Gu, C. Ding, X. Zheng and F. Cao, *ACS Sustainable Chem. Eng.*, 2017, 5, 6548-6556.
40. M. Zhou, B. K. Sharma, P. Liu, H. Xia, J. Xu and J.-c. Jiang, *ACS Sustainable Chem. Eng.*, 2018, 6, 11519-11528.
41. S. Chen, R. Xu, J. Liu, X. Zou, L. Qiu, F. Kang, B. Liu and H. M. Cheng, *Adv. Mater.*, 2019, 31, e1804810.
42. J. T. Grant, C.A. Carrero, F. Goeltl, J. Venegas, P. Mueller, S. P. Burt, S. E. Specht, W. P. McDermott, A. Chieregato and I. Hermans, *Science*, 2016, 354, 1570–1573.
43. C. N. R. Rao and M. Chhetri, *Adv. Mater.*, 2019, 31, e1803668.
44. M. Fan, J. Wu, J. Yuan, L. Deng, N. Zhong, L. He, J. Cui, Z. Wang, S. K. Behera, C. Zhang, J. Lai, B. I. Jawdat, R. Vajtai, P. Deb, Y. Huang, J. Qian, J. Yang, J. M. Tour, J. Lou, C. W. Chu, D. Sun and P. M. Ajayan, *Adv. Mater.*, 2019, 31, e1805778.
45. F. Guo, P. Yang, Z. Pan, X. N. Cao, Z. Xie and X. Wang, *Angew. Chem., Int. Ed.*, 2017, 56, 8231-8235.

46. T. Jin, X. Sang, R. R. Unocic, R. T. Kinch, X. Liu, J. Hu, H. Liu and S. Dai, *Adv. Mater.*, 2018, 30, e1707512.
47. W. Zhu, Z. Wu, G. S. Foo, X. Gao, M. Zhou, B. Liu, G. M. Veith, P. Wu, K. L. Browning, H. N. Lee, H. Li, S. Dai and H. Zhu, *Nat. Commun.*, 2017, 8, 15291.
48. L. Yao, C. Chen, C. G. Yoo, X. Meng, M. Li, Y. Pu, A. J. Ragauskas, C. Dong and H. Yang, *ACS Sustainable Chem. Eng.*, 2018, 6, 14767-14773.
49. L. Shuai, M. T. Amiri, Y. M. Questell-Santiago, F. Heroguel, Y. Li, H. Kim, R. Meilan, C. Chapple, J. Ralph and J. S. Luterbacher, *Science*, 2016, 354, 329-333.
50. B.-C. Zhao, B.-Y. Chen, S. Yang, T.-Q. Yuan, A. Charlton and R.-C. Sun, *ACS Sustainable Chem. Eng.*, 2016, 5, 1113-1122.
51. J.-L. Wen, S.-L. Sun, B.-L. Xue and R.-C. Sun, *Materials*, 2013, 6, 359-391.
52. W. Lei, V. N. Mochalin, D. Liu, S. Qin, Y. Gogotsi and Y. Chen, *Nat. Commun.*, 2015, 6, 8849.
53. L. Zhao, Y. Zhang, L. B. Huang, X. Z. Liu, Q. H. Zhang, C. He, Z. Y. Wu, L. J. Zhang, J. Wu, W. Yang, L. Gu, J. S. Hu and L. J. Wan, *Nat. Commun.*, 2019, 10, 1278.
54. W. Zhu, X. Gao, Q. Li, H. Li, Y. Chao, M. Li, S. M. Mahurin, H. Li, H. Zhu and S. Dai, *Angew. Chem., Int. Ed.*, 2016, 55, 10766-10770.
55. S. Henke, A. Schneemann, A. Wutscher and R. A. Fischer, *J. Am. Chem. Soc.*, 2012, 134, 9464-9474.
56. S. Konar, H. Kalita, N. Puvvada, S. Tantubay, M. K. Mahto, S. Biswas and A. Pathak, *J. Catal.*, 2016, 336, 11-22.
57. Y.-C. Chen, Z.-J. Wu and Y.-K. Hsu, *J. Catal.*, 2019, 370, 224-231.
58. L. Pino, A. Vita, M. Laganà and V. Recupero, *Appl. Catal. B*, 2014, 148-149, 91-105.
59. W. H. Wanna, R. Ramu, D. Janmanchi, Y.-F. Tsai, N. Thiyagarajan and S. S. F. Yu, *J. Catal.*, 2019, 370, 332-346.
60. Z. He, H. Lin, P. He and Y. Yuan, *J. of Catal.*, 2011, 277, 54-63.
61. S. Beniwal, J. Hooper, D. P. Miller, P. S. Costa, G. Chen, S. Y. Liu, P. A. Dowben, E. C. Sykes, E. Zurek and A. Enders, *ACS Nano*, 2017, 11, 2486-2493.
62. S. Shang, P.-P. Chen, L. Wang, Y. Lv, W.-X. Li and S. Gao, *ACS Catalysis*, 2018, 8, 9936-9944.
63. H. Luo and M. M. Abu-Omar, *Green Chem.*, 2018, 20, 745-753.
64. C. K. Nitsos, K. A. Matis and K. S. Triantafyllidis, *ChemSusChem*, 2013, 6, 110-122.
65. J. Ho Seo, H. Jeong, H. W. Lee, C. S. Choi, J. H. Bae, S. M. Lee and Y. S. Kim, *Bioresour. Technol.*, 2019, 275, 368-374.
66. H.-M. Wang, B. Wang, J.-L. Wen, T.-Q. Yuan and R.-C. Sun, *ACS Sustainable Chem. Eng.*, 2017, 5, 11618-11627.
67. G. Wang, X. Liu, B. Yang, C. Si, A. M. Parvez, J. Jang and Y. Ni, *ACS Sustainable Chem. Eng.*, 2019, 7, 10112-10120.
68. C. Li, X. Zhao, A. Wang, G. W. Huber and T. Zhang, *Chem. Rev.*, 2015, 115, 11559-11624.
69. K. Friedel Ortega, R. Arrigo, B. Frank, R. Schlögl and A. Trunschke, *Chem. Mater.*, 2016, 28, 6826-6839.
70. S. Zhao, M. Liu, L. Zhao and L. Zhu, *Ind. Eng. Chem. Res.*, 2018, 57, 5241-5249.
71. A. J. Ragauskas, G. T. Beckham, M. J. Biddy, R. Chandra, F. Chen, M. F. Davis, B. H. Davison, R. A. Dixon, P. Gilna, M. Keller, P. Langan, A. K. Naskar, J. N. Saddler, T. J. Tschaplinski, G. A. Tuskan and C. E. Wyman, *Science*, 2014, 344, 1246843.

72. I. Weinrauch, I. Savchenko, D. Denysenko, S. M. Souliou, H. H. Kim, M. Le Tacon, L. L. Daemen, Y. Cheng, A. Mavrandonakis, A. J. Ramirez-Cuesta, D. Volkmer, G. Schutz, M. Hirscher and T. Heine, *Nat. Commun.*, 2017, 8, 14496.
73. Z.-z. Zhou, M. Liu and C.-J. Li, *ACS Catal.*, 2017, 7, 3344-3348.
74. Y. Xie, J. Wu, G. Jing, H. Zhang, S. Zeng, X. Tian, X. Zou, J. Wen, H. Su, C.-J. Zhong and P. Cui, *Appl. Catal. B*, 2018, 239, 665-676.
75. A. Davó-Quiñonero, D. Lozano-Castelló and A. Bueno-López, *Appl. Catal. B*, 2017, 217, 459-465.
76. G. Yin, Z. Huo, X. Zeng, G. Yao, Z. Jing and F. Jin, *Ind. Eng. Chem. Res.*, 2014, 53, 7856-7865.
77. M. Wang, M. Liu, H. Li, Z. Zhao, X. Zhang and F. Wang, *ACS Catal.*, 2018, 8, 6837-6843.
78. M. Wang, J. Lu, X. Zhang, L. Li, H. Li, N. Luo and F. Wang, *ACS Catal.*, 2016, 6, 6086-6090.